

Photocatalytic Degradation of Bentazon Pesticide by a Fe₂O₃-TiO₂ Composite Catalyst Irradiated by UVA, UVB, and Natural Light

Cristian S. Braga,^a Guilherme G. Bessegato,^b Keiti Maestre,^a Fernando R. Espinoza-Quiñones,^a Helton J. Alves,^c Leandro C. da Silva,^a Renato Eising^d and Reinaldo A. Bariccatti[✉]*,^a

^aCentro de Engenharias e Ciências Exatas, Universidade Estadual do Oeste do Paraná (Unioeste),
Rua da Faculdade, 645, 85903-000 Toledo-PR, Brazil

^bEngenharia de Bioprocessos e Biotecnologia, Universidade Tecnológica Federal do Paraná (UTFPR),
Estrada para Boa Esperança, km 04, 85660-000 Dois Vizinhos-PR, Brazil

^cDepartamento de Engenharia e Ciências Exatas, Universidade Federal do Paraná (UFPR),
Rua Pioneiro, 2153, 85950-000 Palotina-PR, Brazil

^dPrograma de Pós-Graduação em Tecnologias em Biociências (PPGBio),
Universidade Tecnológica Federal do Paraná (UTFPR), R. Cristo Rei, 85902-490 Toledo-PR, Brazil

Environmental pollution by contaminants of emerging concern, among these various pesticides, has been a concern of environmentalists and scientists around the world. Thus, efforts to mitigate the impacts of these substances have been carried out, and the use of advanced oxidation processes, such as photocatalysis, is an alternative. This work sought to synthesize a composite photocatalyst based on iron oxides and titanium dioxide to assess its applicability in degrading the herbicide bentazon (BTZ) by a lamp that simulates the solar spectrum (visible, ultraviolet A and ultraviolet B) and sunlight. Photocatalytic degradation reached 51% in 120 min with a rate constant $k = 0.0058 \text{ min}^{-1}$ when a UV-Vis lamp of 300 W was used. The applicability was demonstrated under sunlight radiation, reaching 38% degradation of a bentazon solution ($4.1 \times 10^{-4} \text{ mol L}^{-1}$) after 320 min. TiO₂ and Fe₂O₃ were synthesized similarly but showed no degradation under the same conditions. Thus, Fe₂O₃-TiO₂ is an inexpensive and non-toxic material capable of efficiently conducting the photocatalytic degradation of organic compounds, such as the bentazon herbicide.

Keywords: photocatalysis, advanced oxidation processes, iron oxide, titanium dioxide

Introduction

Agriculture is responsible for a large contribution to the Brazilian economy, having a great influence on the Gross Domestic Product (GDP) (which accounted for 21.4% in 2019).¹ The growth of agriculture, the improvement of production systems, and the need to increase food production have significantly increased the use of pesticides.²

The release of pesticides into the environment is part of the problem of contaminants of emerging concern (CEC). These compounds may present some risk to the ecosystem, and they are not included in routine monitoring programs, that is, they are not legislated. Many different potential health impacts on humans and the ecosystem may be

caused by CECs, but endocrine disruption is mentioned most frequently, in addition to the potential to cause cancer or have toxic effects on animals and humans.³⁻⁵

Brazil is the fifth-largest pesticide consumer worldwide; however, in relative terms, the use of pesticides *per* cropland area in Brazil is only lower than in China: 5.94 kg *per* ha in Brazil, *versus* 2.54 kg *per* ha in the USA, and 0.62 kg *per* ha in Russia and 13.07 kg *per* ha in China.² Among them, most are herbicides, representing 45% of all commercialized pesticides. The excess of pesticides applied in the plantations contaminates the soil and, due to surface runoff and leaching, the material can be carried, causing contamination of the rivers and underground waters.⁶

The herbicide bentazon (BTZ) (Figure S1, Supplementary Information (SI) section), which belongs to the chemical class of benzotriazinones, can be considered a post-emergent herbicide, being used in Brazil in soybean, corn, and bean crops. In addition to its toxicity,

*e-mail: reinaldo.bariccatti@unioeste.br

Editor handled this article: Jaísa Fernandes Soares

it is a product that has persistence in the environment and is highly mobile, being easily displaced by the soil and can reach the deepest levels of water reservoirs.^{7,8}

During recent decades, many studies have reported the presence of pesticides in surface and even groundwater.⁹⁻¹¹ Nevertheless, wastewater treatment plants (WWTP) are unable to adequately remove most contaminants of emerging concern, including pesticides.^{12,13} In the special case of BTZ, in the WWTP effluent, the concentration was even higher than in the influent, indicating a very poor removal.¹²

The need for more efficient methods of treatment is evident, which can remove not only certain classes of contaminants (such as pesticides) but a wide range of contaminants of emerging concern. Thus, the greatest advances were achieved by advanced oxidative processes (AOPs), based on the generation of highly reactive species, such as the $\cdot\text{OH}$ radicals, which are capable of non-selectively destroying most organic contaminants until their complete mineralization. Among the various forms of generation of $\cdot\text{OH}$ radicals and other reactive species, photocatalysis is based on the use of a semiconductor that, irradiated with photons of energy comparable to its bandgap, promotes the generation of an electron/hole pair; the photogenerated hole in the valence band, when of adequate energy, can oxidize water to hydroxyl radicals or also oxidize contaminants directly on the surface of the photocatalyst.¹⁴⁻¹⁶

Among all transition metal oxides, TiO_2 is recognized as the most researched material in the field of materials science and probably one of the most efficient photocatalysts, despite its relatively high band gap, on the order of 3.2 eV, which requires activation with UV light of about 387 nm.¹⁶ Thus, TiO_2 absorbs only about 5% of the solar rays that reach Earth, limiting its application.¹⁷ Thus, the combination of other semiconductors with lower band gap energies is an alternative. In general, sulfides and nitrides have lower band gap energies but are not as stable in an aqueous medium.¹⁸ As one of the prospective photocatalysts, Fe_2O_3 has become an important material due to its band gap of about 2.3 eV, whose energy can be provided by photons in the visible region of the spectrum with wavelengths smaller than 600 nm (approximately 40% of the solar spectrum).^{17,18} Fe_2O_3 has different crystalline and stoichiometric structures, but hematite ($\alpha\text{-Fe}_2\text{O}_3$) is the most stable state under ambient conditions.¹⁸ Hematite is also stable in aqueous solutions (pH > 3), is low cost, and recyclable.^{18,19} Furthermore, the excitation of electrons to the conduction band triggers the generation of holes in the valence band. The energetic position of the valence band (i.e., its potential) is suitable

for holes to cause oxidation of $\text{H}_2\text{O}/\text{OH}^-$ producing hydroxyl radicals, $\cdot\text{OH}$.^{15,18} However, the wide application of Fe_2O_3 has been restricted by its high electron/hole recombination rate and low diffusion length of charge carriers. To overcome the individual disadvantages of TiO_2 and Fe_2O_3 , a good strategy is the formation of composites or heterostructures, for example.^{17,18,20,21} The formation of a heterojunction between Fe_2O_3 and TiO_2 was shown to enhance photocatalytic activity by improving visible light absorption and promoting the separation of electrons and holes through the interfacial electric field.^{17,20}

The $\text{TiO}_2/\text{Fe}_2\text{O}_3$ composite has several applications such as gas sensors,²² water electrolysis,^{23,24} battery anodes,²⁵ H_2S sensor,²⁶ gaseous acetone sensor,²⁷ activation of persulfates,²⁸ quantum dots,²⁹ nanofibers.³⁰ However, in photocatalysis and photoelectrocatalysis its application is much greater, substances such as cyanide,³¹ methylene blue,³² reduction of 4-nitro-phenol,³³ oxycycline,³⁴ ciprofloxacin,³⁵ phenol,³⁶ Rhodamine-B,³⁷ were photo(electro)catalytically degraded by this material. Among the substances most used to evaluate photocatalytic efficiency is methylene blue dye.³⁸⁻⁴¹ In these works, 67-95% of decolorization is reported for dye solutions with concentrations in the range of 1.0 to 7.8×10^{-5} mol L^{-1} and irradiation time between 60 and 120 min.

Although there are many works in the literature that deal with $\text{Fe}_2\text{O}_3\text{-TiO}_2$ heterojunction, no articles were found that deal with the degradation of the BTZ herbicide with the $\text{Fe}_2\text{O}_3\text{-TiO}_2$ composite or only Fe_2O_3 . Furthermore, the radiation source can not only cause significant changes in degradation efficiency but also impact treatment costs, and the evaluation of the efficiency of the system under sunlight is important. Thus, in this work, we have synthesized composite photocatalysts based on iron(III) oxide (hematite and goethite) and titanium dioxide, evaluating the catalytic activity of the material in the photocatalytic degradation of the herbicide BTZ using UV-Vis radiation.

Experimental

Synthesis of $\text{Fe}_2\text{O}_3/\text{TiO}_2$ composite photocatalyst

Synthesis of the $\text{Fe}_2\text{O}_3/\text{TiO}_2$ photocatalyst was carried out with some modifications to the method used by Zheng *et al.*⁴² First, 0.255 g (1.60×10^{-3} mol) of Fe_2O_3 (Êxodo Científica, Sumaré, Brazil) were added to an Erlenmeyer flask, to which 100 mL of ethanol (Labsynth, Diadema, Brazil) and 45 mL of acetonitrile (Neon, Suzano, Brazil) were added, forming a suspension. This suspension was taken to an ultrasonic bath for 30 min. Then, 0.65 mL of ammonium hydroxide (28%) (Labsynth, Diadema, Brazil) was added to this mixture at room temperature, forming a

suspension at pH 8.0. Then, 2.12 mL (6.91×10^{-3} mol) of titanium isopropoxide (97%) (Sigma Aldrich, Darmstadt, Germany) was added dropwise with agitation. Agitation was maintained for 4.5 h, forming the Fe₂O₃/TiO₂ composite.

The supernatant was removed and then the solid was dried in an oven until a grayish-colored powder was observed, which was then washed with acetonitrile and ethanol. Finally, the particles were dried at 100 °C for 24 h and subjected to a thermal treatment at 360 °C for 3 h.

For comparison purposes, Fe₂O₃ (Êxodo Científica, Sumaré, Brazil) was used without any chemical treatment, and TiO₂ was synthesized according to the previous procedure, but without the addition of Fe₂O₃.

Characterization of materials

X-ray diffraction (XRD) analyzes were performed with D2 Phaser Bruker equipment (Billerica, USA), with Cu-K α 1 radiation (1.54 Å) between 5 and 70°, with an increment of 0.01° and retention time of 0.5 s.

Infrared (FTIR) spectra were recorded by a Frontier PerkinElmer (Waltham, USA) Fourier transform infrared spectrometer. The spectra were obtained on KBr pellets in the range of 4000 to 500 cm⁻¹, with 16 accumulations and a resolution of 1 cm⁻¹, and a sample concentration of approximately 1%. All materials were previously dried at 100 °C for 48 h before analysis.

The differential scanning calorimetry (DSC) measurements were performed by a DSC-60 Shimadzu equipment (Kyoto, Japan), in a nitrogen atmosphere with a flow rate of 10 mL min⁻¹ in the temperature range of 30 to 500 °C.

The morphology of the photocatalysts was investigated by scanning electron microscopy (SEM) performed on a Tescan Vega3 LMU microscope (Brno, Czech Republic), with a resolution of 3 nm, and the images were analyzed with a magnification of 10,000-60,000 \times . Before analysis, the sample was covered with a thin layer of gold.

The percentage of TiO₂ present in the composite material was measured by total reflection X-ray fluorescence (TXRF). Fifteen mg of the sample were weighed and placed in a cryogenic tube with the addition of 5 μ L of gallium standard (Sigma-Aldrich, Gaithersburg, USA) and 2.5 mL of TritonTMX-100 (Sigma-Aldrich, St. Louis, USA). The analyzes were performed on a TXRF S2 PICOFOXTM X-ray fluorescence equipment model, by Bruker.

Photocatalytic degradation of bentazon (BTZ) herbicide

The evaluation of the efficiency of the photocatalysts based on iron(III) oxides was made by experiments on

the degradation of an aqueous solution of BTZ in the concentration of 1.3×10^{-4} mol L⁻¹ (31 mg L⁻¹). For the experiment under solar radiation, the BTZ concentration was 4.1×10^{-4} mol L⁻¹ (98 mg L⁻¹).

The experiments were carried out in a 50 mL borosilicate glass photoreactor positioned inside a cooling jacket and vertically irradiated with an Osram Ultra-Vitalux lamp with a power of 300 W. The system was installed in a dark room and the solution was maintained at 21 °C using a thermostatic bath.

For each photocatalytic degradation experiment, 0.100 g of the photocatalysts were weighed, forming a thin layer of powder at the bottom of the reactor. Then, 20 mL of the bentazon solution was added. The solution containing the contaminant and the photocatalyst was irradiated without stirring, 12 cm from the lamp, and aliquots were taken every 10 min to monitor the degradation.

The degradation of BTZ was monitored by a Shimadzu-1800 UV-Vis spectrophotometer connected to UVProbe software, in the region of 200 to 500 nm with a 10 mm optical path quartz cuvette. After the spectrophotometric analysis, the sample was returned to the reactor. Figure S2 (SI section) shows the representative scheme of the photoreactor.

The light intensity measured during the experiment with solar irradiation started at 22.0×10^3 lumens, the maximum intensity was 37.0×10^3 lumens, and, at the end of the experiment, it was 15.0×10^3 lumens. The intensity was measured in an Instrutemp lux meter, model ITLD 270 (São Paulo, Brazil).

Results and Discussion

Figure 1 shows the X-ray diffractograms of the TiO₂, Fe₂O₃, and Fe₂O₃-TiO₂ composite. The TiO₂ synthesis may result in three distinct crystalline structures: anatase, rutile, and brookite. However, as shown in Figure 1a, TiO₂ powder photocatalyst was most amorphous, as observed by the large band in the diffractogram between 20 and 35°. Furthermore, the diffractogram peaks of bare TiO₂ presented a very low intensity compared to Fe₂O₃-TiO₂ (Figure 1c), confirming its low crystallinity. Concerning Fe₂O₃, there is also a large band with low intensity, indicating low crystallinity. The peaks at 21, 33, and 37° are indexed to the maghemite phase. The red color observed in the solid is characteristic of hematite.

On the other hand, Fe₂O₃-TiO₂ (Figure 1c) presented 45% of crystallinity, which has implications for its photocatalytic activity. Amorphous structures have lower photocatalytic efficiency than crystalline TiO₂ structures, and this low crystallinity can be optimized by thermal

treatment. Peaks at 25, 48, and 51° are characteristic of the structure of the anatase and the peaks at 33 and 37° are the same as observed for Fe₂O₃ in Figure 1b. Similar behavior was observed in the literature by Cornell and Schwertmann.⁴³

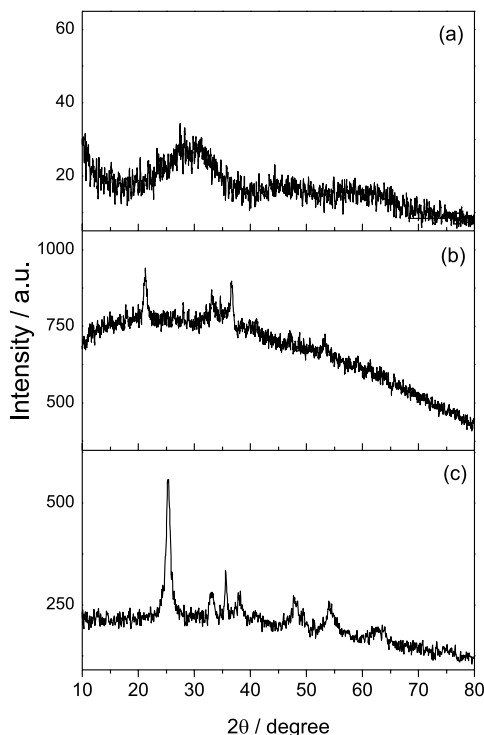


Figure 1. X-ray diffractograms for (a) TiO₂, (b) Fe₂O₃, and (c) Fe₂O₃-TiO₂.

The FTIR spectra for the synthesized inorganic photocatalysts are shown in Figure 2. Initially, the absence of an intense band at 3000 cm⁻¹, related to C–H is indicative of an adequate purity of TiO₂ (Figure 2, curves TiO₂ and Fe₂O₃-TiO₂). The band at 618 cm⁻¹ is related to the axial deformation of Ti–O bonds, while those observed between 1700 and 1250 cm⁻¹ are similar to those observed by Kujawa *et al.*⁴⁴ and are associated with Ti–O vibration modes. The band observed in the region of the 3500–3000 cm⁻¹ are (O–H) groups adsorbed at the surface. Furthermore, the FTIR curves show that the initial iron oxide reagent may contain δ-FeOOH (goethite), in agreement with the literature, showing characteristic stretch bands of the O–H bond (3000 to 3500 cm⁻¹), Figure 2.⁴³

Goethite (α-FeO (OH)) has 36 vibrations, both axial and angular, related to the Fe–O bond, and 12 hydroxy-vibrations; among these, 12 of the Fe–O type vibrations and 5 of the hydroxy type are active in the infrared region. On the other hand, hematite has six active bands in the infrared, all below 800 cm⁻¹. Thus, Fe₂O₃ has crystalline structures in the form of goethite and hematite. DSC

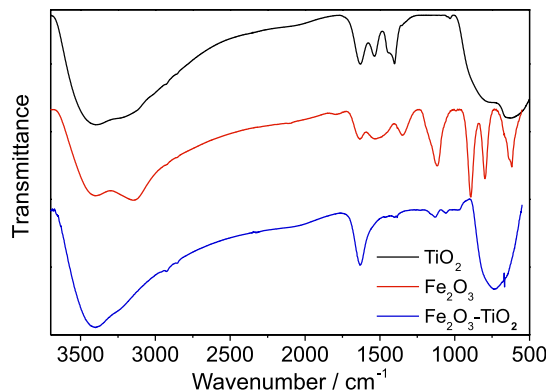


Figure 2. FTIR (KBr) spectra of the photocatalysts: TiO₂, Fe₂O₃, and Fe₂O₃-TiO₂ composite (1.8:1 TiO₂:Fe₂O₃).

analyzes showed characteristic transformations of TiO₂ polymorphs and characteristic transformations of iron oxides.

For the Fe₃O₄-TiO₂ composite, a reduction in the intensities of the goethite bands (between 800 and 1500 cm⁻¹) was observed, as well as an increase in the intensity of the band at 1630 cm⁻¹. Also, the shape of the OH band tended to that seen for the TiO₂ spectrum, accentuating the band by 3200 cm⁻¹, confirming the incorporation of TiO₂ in Fe₂O₃.

The SEM images of the compounds (Figure 3) were magnified 50,000 and 40,000 times for Fe₂O₃ and Fe₂O₃-TiO₂, respectively. The images demonstrate Fe₂O₃ particles with a size of 200 ± 41 nm and Fe₂O₃-TiO₂ with a size of 130 ± 28 nm. Analysis showed that small Fe₂O₃ and Fe₂O₃-TiO₂ particles agglomerate, forming granules of larger diameters, and these formed granules have sizes around 1 μm, sometimes even larger.

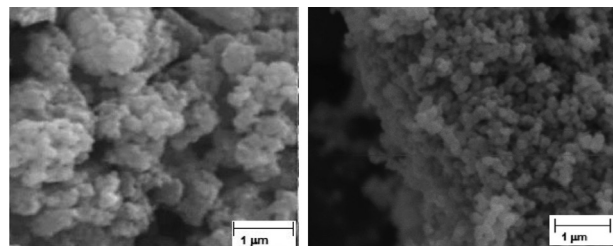


Figure 3. SEM image of Fe₂O₃ with an increase of 50,000× and Fe₂O₃-TiO₂ 40,000×, respectively.

The presence of TiO₂ in the sample was also confirmed by total reflection X-ray fluorescence (TXRF). The presence of titanium in the sample was verified, confirming the formation of the Fe₂O₃-TiO₂ composite. In this case, the titanium mass in the sample was 130 mg g⁻¹ and that of iron was 73.3 mg g⁻¹. According to the preparation methodology, 2.71 mmol of titanium and 1.31 mmol of iron were added *per gram* of sample.

In photocatalytic processes, the lamp plays a vital role in the efficiency of the material. The choice of the Ultra-Vitalux 300 W lamp is due to the emission in the region of UVA and UVB, in addition to visible, similar to that observed in sunlight. According to the manufacturer, this lamp emits 13.6 W, between 315 and 400 nm, and 3.0 W, between 280 and 315 nm, that is, 5.5% of its power in the UV region.

Figure 4 shows the UV-Vis absorption spectrum of a bentazon solution (1.3×10^{-4} mol L⁻¹) and its evolution during photocatalytic treatment. The decrease in the absorption band at 335 and 224 nm indicates the photocatalytic degradation of the target compound by the Fe₂O₃-TiO₂ composite. The observation of isosbestic points at 262 and 300 nm supports the existence of chemical equilibria. These isosbestic points may indicate the formation of bentazon degradation byproducts due to the continuous attack of the \cdot OH radicals. In our work, the trend towards an increase in absorbance at 278 nm stabilizes after 80 min of irradiation. In the first 40 min of irradiation, there was an increase in absorbance of 0.048, while for the last 40 min it increased only 0.008, indicating that the intermediate is also eliminated with increasing irradiation time. Berberidou *et al.*⁴⁵ conducted a complete study of bentazon transformation pathways during photocatalytic degradation. The formation of intermediates as a result of hydrolysis reactions, ring rupture, and addition reactions, such as dimers, hydroxy and/or keto bentazon derivatives, and further oxidized species was detected. Other degradation methods also showed the formation of reaction intermediates.⁴⁶

The bentazon concentrations for each aliquot were calculated using the bentazon molar absorption coefficient and are shown in Table 1, along with the degradation percentage. After 2 h of reaction under controlled conditions, there was a degradation of BTZ, demonstrating that the photocatalytic process with Fe₂O₃-TiO₂ particles

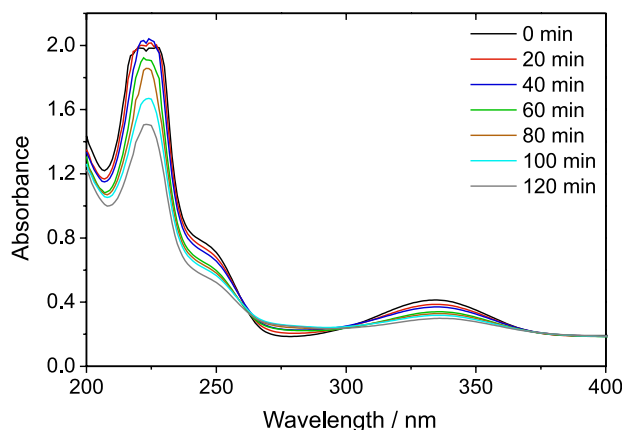


Figure 4. UV-Vis absorption spectra at different treatment times for the photocatalytic degradation of bentazon with the Fe₂O₃-TiO₂ composite catalyst. Conditions: 100 mg of photocatalyst in 20 mL of a 1.3×10^{-4} mol L⁻¹ bentazon solution under irradiation with a 300 W Osram Ultra-Vitalux lamp.

treated at 360 °C is promising for the remediation of contaminated aqueous media.

Photodegradation of bentazon was also attempted with the composite without heat treatment, but no significant changes were observed in the absorption spectra; only the heat-treated photocatalyst showed catalytic activity. The effect of heat treatment on the photocatalytic efficiency of the Fe₂O₃/TiO₂ composite was therefore shown to be important, as already reported in the literature. Nasirian *et al.*⁴⁷ synthesized Fe₂O₃-TiO₂ with different heat treatments (300 to 900 °C) and verified the efficiency of these solids in the degradation of textile dyes. The results indicated that composites treated with temperatures close to 300 °C provided better efficiency in the degradation of selected dyes.

For comparison, bentazon photocatalytic degradation was carried out with iron oxides (Fe₂O₃) and titanium dioxide (TiO₂) prepared by the same method. As shown in Figure S3, no significant changes were observed in the spectra over the degradation time, indicating the absence of a catalytic effect.

Table 1. The decrease in the concentration of bentazon with the time of photocatalytic degradation and the remaining percentage of the pesticide with the Fe₂O₃-TiO₂ composite catalyst (5 g L⁻¹)

time / min	BTZ concentration / (mol L ⁻¹)	Remaining fraction / %	time / min	BTZ concentration / (mol L ⁻¹)	Remaining fraction / %
0	1.32×10^{-4}	100	70	8.53×10^{-5}	64
10	1.27×10^{-4}	96	80	8.23×10^{-5}	62
20	1.16×10^{-4}	88	90	7.95×10^{-5}	60
30	1.12×10^{-4}	85	100	7.59×10^{-5}	57
40	1.07×10^{-4}	81	110	7.15×10^{-5}	54
50	1.02×10^{-4}	77	120	6.45×10^{-5}	49
60	8.88×10^{-5}	67			

BTZ: bentazon.

Schneider *et al.*⁴⁸ performed the degradation of 100% of the herbicide bentazon in 270 min, using TiO₂ and a high-pressure mercury lamp of 125 W. However, the Hg high-pressure lamp has a more intense emission of UVA, UVB, and UVC radiation, making the breakdown of bentazon molecules easier (by photolysis) and also activates TiO₂ in a large extension. In this work, the UV emission produced by the lamp is small, but it has the advantage of a greater correlation with sunlight.

Using the data from Table 1, the kinetics of the pesticide degradation reaction was evaluated using a pseudo-first-order ($\ln(C/C_0)$) model, which provided the best fit (Figure 5). In this kinetic model, mathematical treatment relates the variation in bentazon concentration with the irradiation time.⁴⁸ The curve showed good linearity, with an R² (coefficient of determination) of 0.9965 and a rate

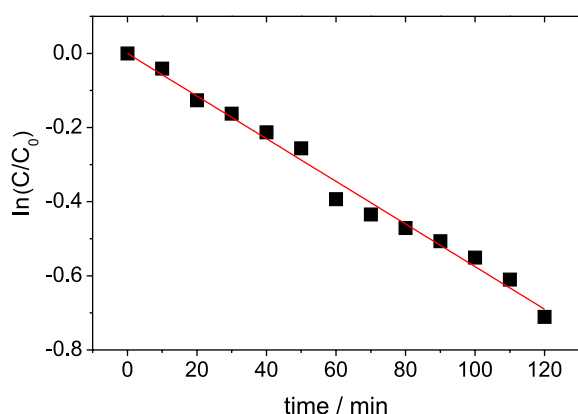


Figure 5. Graph of $\ln(C/C_0)$ versus the time of photocatalytic treatment of a 1.3×10^{-4} mol L⁻¹ solution of bentazon using 5 g L⁻¹ of the Fe₂O₃-TiO₂ composite catalyst, under irradiation of a 300 W UV-Vis lamp.

constant $k = 5.75 \pm 0.94 \times 10^{-3}$ min⁻¹, requiring about 195 min for full degradation.

Subramonian⁴⁹ studied the degradation of effluent from the pulp and paper industry using a Fe₂O₃ and TiO₂ composite and their results were similar to those obtained in this work. The rate constant was 9.2×10^{-3} min⁻¹ and they verified that the catalyst had good performance in the photocatalytic degradation after five reuses (degradation in the range of 80 to 75%). Additionally, the composite has a much more pronounced sedimentation than P25 (TiO₂) and Fe₂O₃ alone, favoring the development of a decantation/precipitation separation system, with the objective of reuse in a pilot project. This reuse is limited only by the characteristics of the catalyst/pollutant, since the surface of the catalyst must have an affinity with the pollutant so that there is adequate distance for the radical attack.

Many of the studies that report photocatalytic degradation with semiconductor oxides make use of Hg lamps, which emit intensely below 280 nm, and this wavelength of solar emission is not observed at sea level. Table 2 shows a comparison of the performances of the photocatalytic degradation of bentazon by several works and their main conditions. Most of these studies use TiO₂ as a photocatalyst for bentazon degradation, and no studies were found applying a Fe₂O₃/TiO₂ composite material. It should be noted, however, that there is no standard for the type of irradiation source and the separation distance between the source and the solution, causing significant variations in the values of the kinetic constant obtained by these works. Therefore, the possibility of activating this photocatalyst with visible light and UVA is an excellent

Table 2. Summary of works dealing with the photocatalytic degradation of bentazon and description of the photocatalyst, main conditions, and reported results

Catalyst	Catalyst concentration / (g L ⁻¹)	k / min ⁻¹	Irradiation source	Initial BTZ concentration / (mg L ⁻¹)	Degradation	Reference
TiO ₂ suspension	1.0	0.067	solar simulator 1000 W	10	95% in 60 min	Kinkennon <i>et al.</i> ⁵⁰
TiO ₂ suspension	1.0	0.160	sunlight	10	95% in 60 min	Kinkennon <i>et al.</i> ⁵⁰
TiO ₂ suspension	0.5	0.053 ^a	solar simulator 1500W	50	ca. 100% in 30 min	Pelizzetti <i>et al.</i> ⁵¹
TiO ₂ nanocrystal	0.5-1.0	0.161	sunlight	32	ca. 100% after 11 kJ L ⁻¹	Seck <i>et al.</i> ⁵²
TiO ₂ nanocrystal	0.2	0.051	Hg lamp 30 W	15	99% in 90 min	Pourata <i>et al.</i> ⁵³
Cu/ZnO (+H ₂ O ₂)	0.5	0.096 ^a	UV C, 125 W	20	ca. 100% in 60 min	Gholami <i>et al.</i> ⁵⁴
C/ZnO	0.5	0.040 ^a	UVA, 9 W	20	ca. 100% in 90 min	Berberidou <i>et al.</i> ⁴⁵
TiO ₂ P25	0.5	0.026 ^a	UVA, 9 W	20	ca. 100% in 90 min	Berberidou <i>et al.</i> ⁴⁵
TiO ₂ nanocrystal	1.0	0.162 ^a	Philips HB 175 60 W	–	63.3%	Seck <i>et al.</i> ⁵²
TiO ₂ P25	1.0	0.079 ^a	Philips HB 175 60 W	–	ca. 85% in 120 min	Seck <i>et al.</i> ⁵⁵
ZnO/TiO ₂	0.5	0.019	UV lamp	20	ca. 80% in 120 min	Ahmed ⁵⁶
TiO ₂ /PMMA	–	0.009	sunlight	10	ca. 100% in 200 min	Mungondori <i>et al.</i> ⁵⁷
TiO ₂ , Aldrich nanoparticles	0.03	0.0116	Hg lamp 125 W	120	ca. 60% in 70 min	Schneider <i>et al.</i> ⁴⁸

^aEstimated values using pseudo-first order model and half-life. BTZ: bentazon; k: reaction rate constant; PMMA: poly(methacrylic acid).

advantage that allows it to be applied on a large scale under solar irradiation.

To prove the photocatalytic activity in the UV-Vis radiation range of the sunlight, the degradation of the bentazon was carried out in open space, under solar irradiation. The study was conducted from 10 to 16 h and the measured luminance during the experiment was 22, 37, and 15 klx at the beginning, in the middle, and at the end of the experiment, respectively. Figure 6 shows the results obtained for the degradation of the bentazon solution using the Fe₂O₃/TiO₂ composite. The characteristic band of the pesticide (at 334 nm) was reduced by 38% after about 320 min of solar irradiation.

This proves that the composite has catalytic activity even under solar irradiation; however, the kinetics under the action of sunlight is difficult to quantify because of the daily light intensity variation and different spectral emission compared to the observed for the laboratory lamp. The increase in absorbance at 278 nm also occurs under solar irradiation. That increase reduces/stabilizes between 90 and 120 min, and after 270 min of irradiation there is a reduction in absorbance in relation to 150 min, indicating the degradation of the herbicide and its by-product.

Control experiments of bentazon degradation under solar irradiation were also carried out: photolysis (without catalyst) and photocatalysis with TiO₂ (synthesized in the same way, but without the presence of Fe). For both cases, there were no significant changes in the absorption spectra of the pesticide.

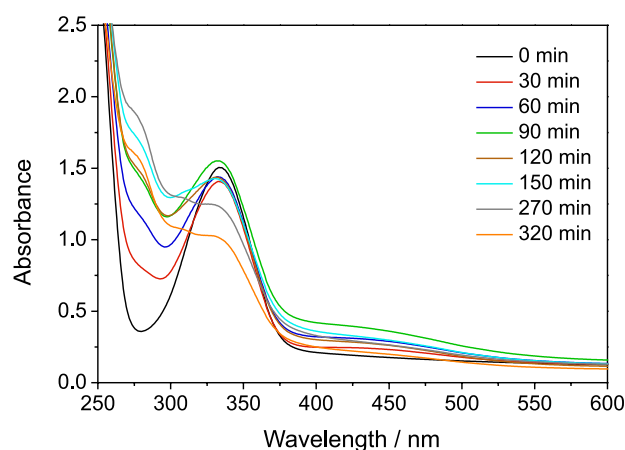


Figure 6. UV-Vis absorption spectra at different treatment times of photocatalytic degradation of an aqueous bentazon solution using the Fe₂O₃-TiO₂ composite catalyst by solar irradiation. Conditions: 100 mg of photocatalyst in 20 mL of a 4.1×10^{-4} mol L⁻¹ (98 mg L⁻¹) bentazon solution under solar irradiation.

Conclusions

The synthesis of a photocatalyst composed of Fe₂O₃-TiO₂ was successfully performed from the titanium

isopropoxide precursor. This material was able to degrade the bentazon herbicide in aqueous solutions under UV-Vis irradiation as verified by the decrease in intensity of the bentazon absorption spectra. Fe₂O₃, TiO₂, and Fe₂O₃-TiO₂ without heat treatment did not show significant degradation when exposed to irradiation; only the composite with heat treatment present photocatalytic efficiency. No literature studies were found with Fe₂O₃-TiO₂ photocatalyst for bentazon degradation and we showed that this possibility proved viable. Under artificial irradiation (Osram Ultra-Vitalux, 300 W), a pseudo-first order kinetics was obtained with $k = 5.75 \pm 0.94 \times 10^{-3}$ min⁻¹, obtaining a half-life in the order of 121 min. Furthermore, degradation of the contaminant has also been demonstrated under sunlight.

Based on these results, it could be possible to coat metal substrates with Fe₂O₃-TiO₂ to assemble low-cost solar reactors for pilot-scale studies. This result is a breakthrough in the search for photocatalysts based on semiconductor oxides, which are cheap, non-toxic, and capable of efficiently conducting the photocatalytic degradation of organic compounds, such as the herbicide bentazon, under sunlight.

Supplementary Information

Supplementary data (chemical structure, photoreactor scheme, and UV-Vis absorption spectra) are available free of charge at <http://jbcs.sbq.org.br> as a PDF file.

Acknowledgments

The authors are grateful for the financial support provided by the Brazilian funding agencies. This study was financed in part by the Coordenação de Aperfeiçoamento de Pessoal de Nível Superior - Brasil (CAPES) - Finance Code 001; Conselho Nacional de Desenvolvimento Científico e Tecnológico - CNPq (process 428014/2018-6); and Fundação Araucária de Apoio ao Desenvolvimento Científico e Tecnológico do Estado do Paraná.

Author Contributions

Cristian S. Braga was responsible for data curation, formal analysis, investigation; Guilherme G. Bessegato for writing original draft, writing-review and editing; Keiti Maestre for data curation, formal analysis, investigation by X-ray fluorescence; Fernando R. F. Espinoza Quinones for data curation, formal analysis, investigation by X-ray fluorescence; Helton J. Alves for data curation, formal analysis, investigation of SEM images; Leandro Couto da Silva for data curation, formal analysis, investigation FTIR and X-ray diffraction; Renato Eising for data curation, formal analysis, investigation FTIR

and X-ray diffraction; Reinaldo A. Bariccatti for conceptualization, funding acquisition, project administration, writing-review and editing.

References

- Center for Advanced Studies on Applied Economics (CEPEA); Brazilian Confederation of Agriculture and Livestock (CNA), Brazilian Agribusiness GDP, <https://www.cepea.esalq.usp.br/en/brazilian-agribusiness-gdp.aspx>, accessed in February 2023.
- Brovini, E. M.; de Deus, B. C. T.; Vilas-Boas, J. A.; Quadra, G. R.; Carvalho, L.; Mendonça, R. F.; Pereira, R. O.; Cardoso, S. J.; *Sci. Total Environ.* **2021**, *771*, 144754. [Crossref]
- Petrie, B.; Barden, R.; Kasprzyk-Hordern, B.; *Water Res.* **2014**, *72*, 3. [Crossref]
- Sauvé, S.; Desrosiers, M.; *Chem. Cent. J.* **2014**, *8*, 15. [Crossref]
- Seibert, D.; Zorzo, C. F.; Borba, F. H.; de Souza, R. M.; Quesada, H. B.; Bergamasco, R.; Baptista, A. T.; Inticher, J. J.; *Sci. Total Environ.* **2020**, *748*, 141527. [Crossref]
- Evgenidou, E.; Fytianos, K.; *J. Agric. Food Chem.* **2002**, *50*, 6423. [Crossref]
- Ali, J. K.; Alhseinat, E.; Abi Jaoude, M.; Al Nashef, I. M.; Adeyemi, I. A.; Aminabhavi, T. M.; Arafat, H. A.; *Chem. Eng. J.* **2022**, *433*, 134596. [Crossref]
- Bessegato, G. G.; Santos, V. P.; Lindino, C. A.; *Quim. Nova* **2012**, *35*, 332. [Crossref]
- Della-Flora, A.; Wielens Becker, R.; Frederigi Benassi, S.; Theodoro Toci, A.; Cordeiro, G. A.; Ibáñez, M.; Portolés, T.; Hernández, F.; Boroski, M.; Sirtori, C.; *Sci. Total Environ.* **2019**, *669*, 248. [Crossref]
- Głinski, D. A.; Purucker, S. T.; Van Meter, R. J.; Black, M. C.; Henderson, W. M.; *Chemosphere* **2018**, *209*, 496. [Crossref]
- de Souza, R. M.; Seibert, D.; Quesada, H. B.; de Jesus Bassetti, F.; Fagundes-Klen, M. R.; Bergamasco, R.; *Process Saf. Environ. Prot.* **2020**, *135*, 22. [Crossref]
- Köck-Schulmeyer, M.; Villagrasa, M.; López de Alda, M.; Céspedes-Sánchez, R.; Ventura, F.; Barceló, D.; *Sci. Total Environ.* **2013**, *458-460*, 466. [Crossref]
- Firouzsalar, N. Z.; Shakerkhatibi, M.; Pourakbar, M.; Yadeghari, A.; Safari, G. H.; Sarbakhsh, P.; *J. Water Process Eng.* **2019**, *29*, 100793. [Crossref]
- Linsebigler, A. L.; Lu, G.; Yates Jr., J. T.; *Chem. Rev.* **1995**, *95*, 735. [Crossref]
- Bessegato, G. G.; Guaraldo, T. T.; de Brito, J. F.; Brugnera, M. F.; Zannoni, M. V. B.; *Electrocatalysis* **2015**, *6*, 415. [Crossref]
- Paramasivam, I.; Jha, H.; Liu, N.; Schmuki, P.; *Small* **2012**, *8*, 3073. [Crossref]
- Palanisamy, B.; Babu, C. M.; Sundaravel, B.; Anandan, S.; Murugesan, V.; *J. Hazard Mater.* **2013**, *252-253*, 233. [Crossref]
- Mishra, M.; Chun, D.-M.; *Appl. Catal., A* **2015**, *498*, 126. [Crossref]
- Hitam, C. N. C.; Jalil, A. A.; *J. Environ. Manage.* **2020**, *258*, 110050. [Crossref]
- Peng, L.; Xie, T.; Lu, Y.; Fan, H.; Wang, D.; *Phys. Chem. Chem. Phys.* **2010**, *12*, 8033. [Crossref]
- Beydoun, D.; Amal, R.; Low, G. K. C.; McEvoy, S.; *J. Phys. Chem. B* **2000**, *104*, 4387. [Crossref]
- Mei, H.; Zhou, S.; Lu, M.; Zhao, Y.; Cheng, L.; *Ceram. Int.* **2020**, *46*, 18675. [Crossref]
- Vattikuti, S. V. P.; Devarayapalli, K. C.; Reddy Nallabala, N. K.; Nguyen, T. N.; Nguyen Dang, N.; Shim, J.; *J. Phys. Chem. Lett.* **2021**, *12*, 5909. [Crossref]
- Mohamed, R. M.; Kadi, M. W.; Ismail, A. A.; *Ceram. Int.* **2020**, *46*, 15604. [Crossref]
- Zuniga, L.; Gonzalez, G.; Chavez, R. O.; Myers, J. C.; Lodge, T. P.; Alcoutlabi, M.; *Appl. Sci.* **2019**, *9*, 4032. [Crossref]
- Xu, Z.; Liu, H.; Tong, X.; Shen, W.; Chen, X.; Bloch, J.-F.; *J. Mater. Sci. Mater. Electron.* **2019**, *30*, 12695. [Crossref]
- Wang, C.; Wang, Y.; Cheng, P.; Xu, L.; Dang, F.; Wang, T.; Lei, Z.; *Sens. Actuators, B* **2021**, *340*, 129926. [Crossref]
- Zhang, X.; Duan, J.; Tan, Y.; Deng, Y.; Li, C.; Sun, Z.; *Sep. Purif. Technol.* **2022**, *293*, 121123. [Crossref]
- Zhang, J.; Kuang, M.; Wang, J.; Liu, R.; Xie, S.; Ji, Z.; *Chem. Phys. Lett.* **2019**, *730*, 391. [Crossref]
- Liu, H.; Zhang, Z.-G.; Wang, X.-X.; Nie, G.-D.; Zhang, J.; Zhang, S.-X.; Cao, N.; Yan, S.-Y.; Long, Y.-Z.; *J. Phys. Chem. Solids* **2018**, *121*, 236. [Crossref]
- Eskandari, P.; Farhadian, M.; Solaimany Nazar, A. R.; Jeon, B. H.; *Ind. Eng. Chem. Res.* **2019**, *58*, 2099. [Crossref]
- Mansour, H.; Omri, K.; Bargougui, R.; Ammar, S.; *Appl. Phys. A: Mater. Sci. Process* **2020**, *126*, 1. [Crossref]
- Anusuya, N.; Pragathiswaran, C.; Thulasi, G.; *Mater. Today: Proc.* **2021**, *37*, 3759. [Crossref]
- Liu, M.; Yu, S.; Hou, L.-a.; Hu, X.; *J. Mater. Sci.: Mater. Electron.* **2019**, *30*, 9087. [Crossref]
- Wang, F.; Yu, X.; Ge, M.; Wu, S.; *Chem. Eng. J.* **2020**, *384*, 123381. [Crossref]
- Bouziani, A.; Park, J.; Ozturk, A.; *J. Photochem. Photobiol., A* **2020**, *400*, 112718. [Crossref]
- Zhou, Z.; Yin, H.; Zhao, Y.; Zhang, J.; Li, Y.; Yuan, J.; Tang, J.; Wang, F.; *Catalysts* **2021**, *11*, 396. [Crossref]
- Abbas, N.; Shao, G. N.; Haider, M. S.; Imran, S. M.; Park, S. S.; Kim, H. T.; *J. Ind. Eng. Chem.* **2016**, *39*, 112. [Crossref]
- Cao, X.; Luo, S.; Liu, C.; Chen, J.; *Adv. Powder Technol.* **2017**, *28*, 993. [Crossref]
- Ahmed, M. A.; El-Katori, E. E.; Gharni, Z. H.; *J. Alloys Compd.* **2013**, *553*, 19. [Crossref]
- Li, R.; Jia, Y.; Bu, N.; Wu, J.; Zhen, Q.; *J. Alloys Compd.* **2015**, *643*, 88. [Crossref]
- Zheng, L.; Xu, H.; Pi, F.; Zhang, Y.; Sun, X.; *RSC Adv.* **2016**, *6*, 87273. [Crossref]

43. Cornell, M. R.; Schwertmann, U.; *The Iron Oxides: Structure, Properties, Reactions, Occurrences and Uses*; 2nd ed.; John Wiley & Sons: Weinheim, 2006.
44. Kujawa, J.; Cerneaux, S.; Kujawski, W.; *Colloids Surf., A* **2014**, *447*, 14. [Crossref]
45. Berberidou, C.; Kitsiou, V.; Kazala, E.; Lambropoulou, D. A.; Kouras, A.; Kosma, C. I.; Albanis, T. A.; Poullos, I.; *Appl. Catal., B* **2017**, *200*, 150. [Crossref]
46. Ania, C. O.; Béguin, F.; *Water Res.* **2007**, *41*, 3372. [Crossref]
47. Nasirian, M.; Bustillo-Lecompte, C. F.; Mehrvar, M.; *J. Environ. Manage.* **2017**, *196*, 487. [Crossref]
48. Schneider, M. V.; Rosa, M. F.; Lobo, V. S.; Bariccatti, R. A.; *Eng. Sanit. Ambient.* **2014**, *19*, 61. [Crossref]
49. Subramonian, W.; Wu, T. Y.; Chai, S.-P.; *J. Environ. Manage.* **2017**, *187*, 298. [Crossref]
50. Kinkennon, A. E.; Green, D. B.; Hutchinson, B.; *Chemosphere* **1995**, *31*, 3663. [Crossref]
51. Pelizzetti, E.; Maurino, V.; Minero, C.; Zerbinati, O.; Borgarello, E.; *Chemosphere* **1989**, *18*, 1437. [Crossref]
52. Seck, E. I.; Doña-Rodríguez, J. M.; Fernández-Rodríguez, C.; Portillo-Carrizo, D.; Hernández-Rodríguez, M. J.; González-Díaz, O. M.; Pérez-Peña, J.; *Solar Energy* **2013**, *87*, 150. [Crossref]
53. Pourata, R.; Khataee, A. R.; Aber, S.; Daneshvar, N.; *Desalination* **2009**, *249*, 301. [Crossref]
54. Gholami, M.; Jonidi-Jafari, A.; Farzadkia, M.; Esrafil, A.; Godini, K.; Shirzad-Siboni, M.; *J. Environ. Manage.* **2021**, *294*, 112962. [Crossref]
55. Seck, E. I.; Doña-Rodríguez, J. M.; Fernández-Rodríguez, C.; González-Díaz, O. M.; Araña, J.; Pérez-Peña, J.; *Chem. Eng. J.* **2012**, *203*, 52. [Crossref]
56. Ahmed, S.; *J. Phys.: Conf. Ser.* **2019**, *1310*, 012015. [Crossref]
57. Mungondori, H. H.; Tichagwa, L.; Katwire, D. M.; Aoyi, O.; *Iran. Polym. J.* **2016**, *25*, 135. [Crossref]

Submitted: July 12, 2022

Published online: March 16, 2023

